Catalysis Today xxx (2016) xxx–xxx

Contents lists available at ScienceDirect

Catalysis Today

journal homepage: www.elsevier.com/locate/cattod

Catalytic transfer hydrogenation of biomass-derived levulinic acid and its esters to γ-valerolactone over ZrO_2 catalyst supported on SBA-15 silica

Yasutaka Kuwahara[a,b,*], Wako Kaburagi[c], Yohsuke Osada[c], Tadahiro Fujitani[c], Hiromi Yamashita[a,b,*]

[a] Division of Materials and Manufacturing Science, Graduate School of Engineering, Osaka University, 2-1 Yamada-oka, Suita, Osaka 565-0871, Japan
[b] Unit of Elements Strategy Initiative for Catalysts & Batteries (ESICB), Kyoto University, Katsura, Kyoto 615-8520, Japan
[c] Interdisciplinary Research Center for Catalytic Chemistry, National Institute of Advanced Industrial Science and Technology (AIST), 1-1 Higashi, Tsukuba, Ibaraki, Japan

ARTICLE INFO

Article history:
Received 10 January 2016
Received in revised form 10 March 2016
Accepted 5 May 2016
Available online xxx

Keywords:
Biomass conversion
Levulinic acid
γ-Valerolactone
Catalytic transfer hydrogenation
Mesoporous silica

ABSTRACT

A series of ZrO_2 catalysts supported on mesoporous SBA-15 silica were synthesized and examined as catalysts in the production of γ-valerolactone (GVL) from biomass-derived levulinic acid and its esters *via* a catalytic transfer hydrogenation (CTH) using several alcohols as hydrogen donors. Among the catalysts examined, ZrO_2 supported on high-surface-area SBA-15 silica bearing highly-dispersed zirconium species exhibited the highest catalytic activity, of which reaction rate was 1.7 times higher than that of the conventional bulk ZrO_2 catalyst. Zr K-edge XAFS analysis revealed that Zr^{4+}-oxide species with a low-coordination state anchored on silica surface is the dominant active species. Such a Zr species efficiently converted levulinic acid and its esters to GVL (~95% yields) under mild reaction conditions (150 °C, 1.0 MPa Ar), and was reusable over multiple catalytic cycles without significant loss of catalytic performances. Comparative experiments, combined with detailed characterizations using NH_3/CO_2-TPD and *in-situ* FTIR, proposed a plausible reaction mechanism where basic Zr—OH site triggers the CTH reaction involving a six-member ring transition state.

1. Introduction

Due to the depletion of fossil fuel resources, rapid increase of anthropogenic CO_2 emissions and the associated deterioration of environmental quality, the search for renewable resources is a matter of worldwide concern. Lignocellulosic biomass is a promising feedstock for the production of fuels and chemicals, since it is an abundant, inexpensive and carbon-neutral source and is available worldwide. Recent efforts in the catalysis field have found a number of promising approaches for the catalytic transformation of lignocellulosic biomass to produce various chemicals industrially valuable (so-called "biomass refinery") [1–7]. Among a wide range of chemicals obtained from lignocellulosic biomass, γ-valerolactone (GVL) has been identified as one of the most alluring platform molecules [8,9], since it can be used as a fuel additive, solvent for biomass processing [10], as well as a versatile intermediate for the production of olefins [11], polymers [12,13], and other value-added chemicals [14,15]. Moreover, GVL can be used as a precursor to produce various liquid hydrocarbon fuels suitable for gasoline, diesel and aviation kerosene *etc.* [16,17].

GVL is typically obtained through the reduction of levulinic acid (LA) and its esters, which are intermediate molecules produced by acid-catalyzed solvolysis of various carbohydrate fractions of lignocelluloses, such as glucose, fructose, as well as 5-hydroxymethylfurfural (HMF), in water [18–20] and alcohols [21–25], respectively. There are two possible pathways to produce GVL from LA and its esters; (i) the hydrogenation (using molecular H_2) and (ii) the catalytic transfer hydrogenation (CTH) (using alcohols). The former hydrogenation reaction is conventionally performed over homogeneous/heterogeneous noble metal catalysts (such as Pd [26–28], Pt [26], Ru [29–34], Ir [35]), which allow GVL production with high yields. However, the noble metal catalysts are expensive and inevitably suffer from deactivation, and the systems require flammable, high-pressure H_2 (>30 bar), limiting large-scale operation requisite for biomass refinery. In contrast, the latter CTH

* Corresponding authors at: Division of Materials and Manufacturing Science, Graduate School of Engineering, Osaka University, 2-1 Yamada-oka, Suita, Osaka 565-0871, Japan.
E-mail addresses: kuwahara@mat.eng.osaka-u.ac.jp (Y. Kuwahara), yamashita@mat.eng.osaka-u.ac.jp (H. Yamashita).

http://dx.doi.org/10.1016/j.cattod.2016.05.016
0920-5861/

process is a better alternative route for energy-saving and scalable production of GVL, since the reaction proceeds under milder conditions using low-cost metal oxides as catalysts and alcohols as cheaper and safer H-donors [36,37]. In addition, in an ideal process for the production of levulinate derivatives from lignocellulosic carbohydrates, use of alcohol media (methanol and ethanol *etc.*) is preferred rather than water because of higher yields and an easier isolation of the produced levulinate esters than LA [21–23]. Furthermore, the alcohols spent at this stage are supposed to be reused as H-donors in the following CTH process. Thus, CTH process would meet both the economic and technical requirements needed for GVL production from biomass.

Regarding the production of GVL *via* a CTH process, several catalytic systems have recently been reported. A pioneering work was done by Chia and Dumesic et al. who reported a CTH process to convert LA and its esters into GVL using bulk ZrO_2 and *iso*-propanol/*iso*-butanol as H-donors at 150 °C under pressurized inert gas conditions (300 psig He) [38]. Sun and Lin et al. reported that hydrated zirconia acts as an efficient heterogeneous catalyst for a CTH reaction of ethyl levulinate in a supercritical ethanol at around 250 °C [39,40]. However, these works revealed that bulk zirconia catalysts hold critical drawbacks such as high catalyst loading, relatively high reaction temperature/pressure, moderate GVL selectivity and appreciable catalyst deactivation during the reaction. Recently, Román-Leshkov et al. and Chuah et al. reported that microporous molecular sieve bearing isolated Zr sites (Zr-beta) is a more effective catalyst compared with bulk zirconia [41,42], giving us an idea that dispersed Zr sites immobilized on oxide support can afford increased catalytic activities. According to these works, we recently reported that low-cost and readily-prepared silica-supported ZrO_2 catalyst works as a better alternative for CTH reaction of LA and its esters under relatively mild reaction conditions (150 °C, 1.0 MPa of Ar) [43]. Although the catalytic activity was found to be significantly influenced by altering type of the oxide supports, a deep insight to the activity–structure relationship has not been obtained, and the local structure of the active Zr species and the associated reaction mechanism have not fully been understood.

In this study, an array of ZrO_2 catalyst supported on SBA-15 silica were prepared and examined in CTH reaction of LA and its esters to produce GVL. The structure of the catalysts, including local information concerning the overall porous properties and the state of the supported Zr atoms, were investigated in detail to draw a relationship between the structure and catalytic performances and to identify the real active Zr species. Furthermore, detailed characterizations using NH_3/CO_2-TPD and *in-situ* FTIR were performed to propose a plausible reaction mechanism. In addition, the scope of substrates and alcohols as well as catalyst recyclability was also investigated to demonstrate broad applicability of the catalyst.

2. Experimental

2.1. Materials

All commercially available chemical reagents for material synthesis and catalytic tests were purchased from Wako Pure Chemical Ind., Ltd. unless otherwise noted and used without further purification. A pure siliceous SBA-15 was prepared by a hydrothermal synthesis method using Pluronic P123® (PEO_{20}-PPO_{70}-PEO_{20}, Aldrich, M_W = 5800) as an organic template and tetraethoxyorthosilicate (TEOS) as a silicon source according to the previous literature [44]. A pure siliceous MCM-41 was prepared by a hydrothermal synthesis method using cetyltrimethylammonium bromide (CTAB) as an organic template and TEOS as a silicon source with the molar ratio of Si: NH_3: CTAB: H_2O = 1.0: 3.3: 0.1: 66 [45].

2.2. Catalyst preparation

Supported ZrO_2 catalysts were prepared by *in-situ* hydrolysis of zirconium *n*-butoxide ($Zr(O^nBu)_4$, 70% in *n*-butanol, Tokyo Chemical Industry Co., Ltd.) on oxide support in an organic solvent according to a previously reported method [43]. In a typical synthesis, SBA-15 silica was carefully treated at 150 °C under vacuum to remove physisorbed water. To a glass flask containing dried SBA-15 support (2.0 g), 60 mL of 2-propanol containing desired amount of $Zr(O^nBu)_4$ was added, followed by stirring at room temperature for 1 h in Ar atmosphere and further stirring at 80 °C for 5 h in air. The obtained suspension was filtered, washed with ethanol, and dried at 100 °C overnight, and was finally calcined in air at 400 °C for 6 h to afford ZrO_2(*X*)/SBA-15, where *X* represents the ZrO_2 content in the initial synthesis gel. Other types of silica (MCM-41 and fumed SiO_2) were also used as supports for ZrO_2.

For comparison, pure ZrO_2 was synthesized by a precipitation method under basic conditions; briefly, a total of 13.5 g of $ZrO(NO_3)_2{\cdot}2H_2O$ (99.5%) was dissolved in 500 mL of deionized water, followed by precipitation at pH 9.0 with 10% NH_3 solution with vigorous stirring and aging at room temperature for 48 h. The obtained precipitate was filtered, thoroughly washed with deionized water, dried at 100 °C overnight, and was finally calcined in air at 400 °C for 6 h to give pure ZrO_2 [25].

2.3. Characterization

X-ray diffraction (XRD) measurements were performed using a Bruker AXS D8 Advance X-ray diffractometer with CuKα radiation (λ = 1.54056 Å). Nitrogen adsorption–desorption isotherms were measured at −196 °C by using Micromeritics ASAP2020 system. Prior to the measurements, the samples were degassed at 300 °C under vacuum for 4 h to remove physisorbed water. The specific surface area was calculated by the BET (Brunauer–Emmett–Teller) method by using adsorption data ranging from p/p_0 = 0.05 to 0.30. The pore size distributions were obtained from the adsorption branches of the nitrogen isotherms by the BJH (Barret–Joyner–Halenda) method. Transmission electron microscope (TEM) images were taken with a FEI TITAN80-300 operated at 200 kV. Thermal gravimetric analysis and differential thermal gravimetric analysis (TG/DTG) were carried out on a MAC Science TG-DTA2000 S system under a flow of air (50 mL/min) with a heating rate of 10 °C/min.

Zr K-edge X-ray absorption fine structure (XAFS) measurement was performed in transmission mode at room temperature at the BL01B1 beam line of SPring-8, Japan. A Si(311) single crystal was used to obtain the monochromated X-ray beam. The Fourier transformation of k^3-weighted normalized EXAFS data (FT-EXAFS) from *k* space to *r* space was performed over the range $3.0 < k\ (Å^{-1}) < 13.0$ to obtain the radial structure function (RDF). For the curve-fitting analysis, the empirical phase shift and amplitude functions for Zr—O and Zr···Zr were extracted from the data for monoclinic ZrO_2. The analysis of the XAFS data was performed by using Rigaku REX2000 software.

The acidity and basicity of the samples were quantified by temperature programmed desorption of NH_3 (NH_3-TPD) and CO_2 (CO_2-TPD), respectively, using a BELCAT-B system (BEL Japan, Inc.). Approximately 100 mg of sample mounted in a quartz tube was pretreated at 600 °C in a He gas flow (50 mL/min) for 1 h, allowed to cool to 50 °C, and subsequently exposed to either 5% NH_3/He gas or 100% CO_2 gas (50 mL/min) for 1 h. After being flushed with He for 0.5 h to eliminate weakly-adsorbed NH_3/CO_2 molecules, TPD was carried out between 50 and 600 °C under a He flow (30 mL/min) with a ramping rate of 10 °C/min, and the desorbed NH_3/CO_2 was detected by a thermal conductivity detector.

Please cite this article in press as: Y. Kuwahara, et al., Catalytic transfer hydrogenation of biomass-derived levulinic acid and its esters to γ-valerolactone over ZrO_2 catalyst supported on SBA-15 silica, Catal. Today (2016), http://dx.doi.org/10.1016/j.cattod.2016.05.016

In-situ FTIR spectroscopy measurement was performed by using a Cary 670-IR instrument (Agilent technology, Inc.) in the spectral range 4000–1000 cm^{-1}. Approximately 5 mg of sample was pressed into a self-supported wafer (ϕ10 mm). The wafer loaded into a high-vacuum transmission FTIR cell was pretreated at 400 °C under a He flow (100 mL/min) for 1 h, allowed to cool to 180 °C, and then the baseline spectrum was collected. After exposing to a flow of 25 mbar 2-propanol in He (100 mL/min) for 1 h, FTIR difference spectra of 2-propanol adsorbed on the sample were collected under flushing in a He flow (100 mL/min) by subtracting the baseline spectrum from the each collected spectrum.

2.4. Procedures for catalytic reactions

In a typical reaction, a reaction mixture containing catalyst (40 mg as ZrO_2), substrate (2 mmol), and alcohol (10 mL) was charged into a 60 mL cylindrical stainless steel high-pressure reactor (EYELA, Inc.) equipped with a bourdon pressure gauge, which was then sealed, purged and pressurized with 1.0 MPa of Ar and then heated to 150 °C. During the reaction, magnetic stirring at 600 rpm was continued. After the predetermined reaction time, the reactor was cooled to room temperature and the liquid products recovered from the reaction mixture were analyzed by a gas chromatograph (Shimadzu GC-14B) with a frame ionization detector equipped with a capillary column (ULBON HR-20 M; 0.53 mm × 30 m; Shinwa Chemical Ind., Ltd.). Conversion of substrate and yields of products were quantified using biphenyl as an internal standard. To assess the catalyst reusability, the spent catalyst was retrieved from the reaction mixture by filtration, washed with acetone, dried at 100 °C and then subjected to multiple catalytic runs (for detailed procedures for catalyst reusability test, see the Supplementary Information).

3. Results and discussion

3.1. Structural analysis

For the synthesis of silica-supported ZrO_2 catalysts, *in-situ* hydrolysis method of zirconium *n*-butoxide was employed, so as to obtain the catalysts with desired ZrO_2 content. The ZrO_2 content was controlled by simply varying the amount of zirconium *n*-butoxide precursor in the initial gel to obtain SBA-15-supported ZrO_2 catalysts with 9.8 wt% (ZrO_2(10)/SBA-15), 19.4 wt% (ZrO_2(20)/SBA-15), 32.7 wt% (ZrO_2(35)/SBA-15), 49.7 wt% (ZrO_2(50)/SBA-15) and 59.2 wt% (ZrO_2(60)/SBA-15) ZrO_2 loading (Table 1). Fig. 1 shows XRD patterns of ZrO_2/SBA-15 materials with varied ZrO_2 contents. Low angle XRD patterns of ZrO_2/SBA-15 materials all exhibited well-defined diffraction planes associated with 2D hexagonal mesoporous structure (*P6 mm* symmetry) which are similar to those of the parent SBA-15. The intensities of the peak at around $2\theta = 0.9°$ ascribed to the (100) diffraction gradually decreased as increasing the ZrO_2 content, while the lattice paramater a_0, which represents the distance between the mesopores, mostly remained unchanged (Table 1), indicating a blockage of mesopores by the incorporation of ZrO_2. In high angle XRD patterns, no diffraction patterns were observed for the samples with ZrO_2 contents lower than 20 wt%, suggesting that Zr species is existing as highly-dispersed Zr species or as amorphous zirconia. A similar result was observed for ZrO_2 supported on fumed silica and MCM-41 silica (see Fig. A in the Supplementary Information). On the other hand, the samples with higher ZrO_2 content (ZrO_2 > 35 wt%) exhibited diffraction patterns indexed to tetragonal ZrO_2 phase ($2\theta = 30.2$, 35.2, 50.4 and 60.1°), representing the formation of aggregated ZrO_2 species.

The porous properties of the catalysts were investigated by N_2 physisorption measurement. The parent SBA-15 displays a type IV nitrogen adsorption-desorption isotherm with a clear capillary condensation at around $p/p_0 = 0.7$ due to the presence of periodically-aligned mesopore channel systems (Fig. 2(A) (a)). The isotherms of ZrO_2/SBA-15 materials showed decreased quantities of adsorbed N_2 and less defined hysteresis loops (Fig. 2(A)–(d)), indicating subpar porous qualities (for N_2 physisorption data of ZrO_2(10)/MCM-41 and ZrO_2(10)/SiO_2, see Fig. B). The textural properties obtained from XRD measurement and N_2 adsorption isotherms are tabulated in Table 1. Along with the increase of ZrO_2 content from 0 to 59.2 wt%, the specific surface area (S_{BET}) and total pore volume (V_{total}) linearly reduced (S_{BET}: from 1040 to 475 m^2/g, V_{total}: from 1.34 to 0.39 cm^3/g). Nonetheless, the materials still had large surface areas and pore volumes as to be regarded as mesoporous materials. The pore size distribution curves calculated from the N_2 adsorption data showed broader pore size distributions as increasing the ZrO_2 content (Fig. 2(B)). The average pore diameter (D_p) linearly decreased from 8.5 to 5.8 nm as the ZrO_2 content increases from 0 to 59.2 wt%, and consequently the thickness of silica wall (T_w) increased from 5.5 nm to 8.2 nm. The mesoporous structure of SBA-15 was confirmed by TEM images. ZrO_2(10)/SBA-15 showed a similar morphological feature to that of bare SBA-15, representing the retention of the original mesopore structure (Fig. 3(a) and (b)). On the other hand, ZrO_2(35)/SBA-15 and ZrO_2(60)/SBA-15 showed extra-framework aggregated ZrO_2 particles (Fig. 3(c) and (d), respectively). These combined characterization results demonstrate that Zr species are dominantly deposited inside the pore channels with uniform distribution at lower ZrO_2 loading levels, but introduction of an excess amount of Zr (>35 wt%) leads to a formation of extra-framework aggregated ZrO_2 particles and accordingly results in reduced mesoporosity.

The thus synthesized catalysts were tested for CTH reaction of methyl levulinate (ML) using 2-propanol as a H-donor at 150 °C under 1.0 MPa of Ar. The amount of ZrO_2 introduced to the reactor was fixed to be the same in all cases to compare catalytic activities per amount of ZrO_2. When 2-propanol was used as a H-donor, GVL was produced as a major product, and transesterification product (*i.e.*, isopropyl levulinate ester) and hydrogenated compounds (*i.e.*, 4-hydroxypentanoic acid methyl/isopropyl esters (4-HPE)) were produced as by-products. Appreciable amounts of acetone and methanol were also detected, elucidating that the reaction proceeds *via* a CTH reaction and the following dealcoholization steps as illustrated in Scheme 1, where transesterifications of ML and 4-HPE with alcohols take place as side reactions. As shown in Table 2, a series of SBA-15-supported ZrO_2 catalysts showed higher catalytic activities (Entries 1–5) than bulk ZrO_2 (Entry 8), but increasing ZrO_2 content from 9.8 to 49.7 wt% resulted in a gradual activity decrease (for reaction kinetics data, see Fig. C). At a fixed loading level (10 wt%) of ZrO_2, SBA-15 was the most effective support to achieve high GVL production rate among three types of silica support (SBA-15, MCM-41 and fumed silica) (*cf.* Entries 1, 6 and 7). ZrO_2(10)/SBA-15 (S_{BET} = 810 m^2/g, D_p = 7.7 nm) afforded >99.5% conversion and 91% GVL yield at 3 h of reaction, of which reaction rate was 1.7 times higher than that of the conventional bulk ZrO_2 (55% conversion and 53% GVL yield). ZrO_2(10)/MCM-41 (S_{BET} = 783 m^2/g, D_p = 2.9 nm) and ZrO_2(10)/SiO_2 (S_{BET} = 250 m^2/g) gave almost similar activities (98% conversions and 87–89% GVL yield) under the same conditions, while they have totally different porous structures and surface area. These experimental results led us to a hypothesis that unique local structure of the Zr atoms highly-dispersed on silica support might be responsible for achieving a high catalytic activity, rather than the textural properties of silica supports such as topology, pore size and surface area.

Please cite this article in press as: Y. Kuwahara, et al., Catalytic transfer hydrogenation of biomass-derived levulinic acid and its esters to γ-valerolactone over ZrO_2 catalyst supported on SBA-15 silica, Catal. Today (2016), http://dx.doi.org/10.1016/j.cattod.2016.05.016

Table 1
Textural properties of silica-supported ZrO_2 catalysts.

Sample	ZrO_2 content[a] (wt%)	XRD		N_2 physisorption			
		d_{100}[b] (nm)	a_0[c] (nm)	S_{BET}[d] (m^2/g)	V_{total}[e] (cm^3/g)	D_p[f] (nm)	T_w[g] (nm)
SBA-15	–	9.9	14.0	1040	1.34	8.5	5.5
ZrO_2(10)/SBA-15	9.8	9.9	14.0	810	1.03	7.7	6.3
ZrO_2(20)/SBA-15	19.4	9.6	13.6	733	0.83	7.1	6.5
ZrO_2(35)/SBA-15	32.7	9.6	13.6	724	0.75	6.7	6.9
ZrO_2(50)/SBA-15	49.7	9.6	13.6	597	0.57	6.3	7.3
ZrO_2(60)/SBA-15	59.2	9.9	14.0	475	0.39	5.8	8.2
MCM-41	–	5.6	7.9	923	0.86	2.9	5.0
ZrO_2(10)/MCM-41	9.7	5.6	7.9	783	0.65	2.9	5.0
SiO_2	–	N.D.	N.D.	279	0.60	N.D.	N.D.
ZrO_2(10)/SiO_2	9.6	N.D.	N.D.	250	0.71	N.D.	N.D.
ZrO_2	100	N.D.	N.D.	112	0.29	N.D.	N.D.

[a] Molar ratio determined by EDX.
[b] Calculated from Bragg's equation: $2d_{100} \sin\theta = n\lambda$ ($\lambda = 0.154056$ nm).
[c] Lattice parameter defined by $a_0 = 2d_{100}/\sqrt{3}$ assuming hexagonal structure.
[d] Specific surface area calculated by BET method from N_2 adsorption data.
[e] Total pore volume at $p/p_0 = 0.99$.
[f] Average pore diameter determined by BJH method.
[g] Wall thickness defined by $T_w = a_0 - D_p$. N.D. = Not determined.

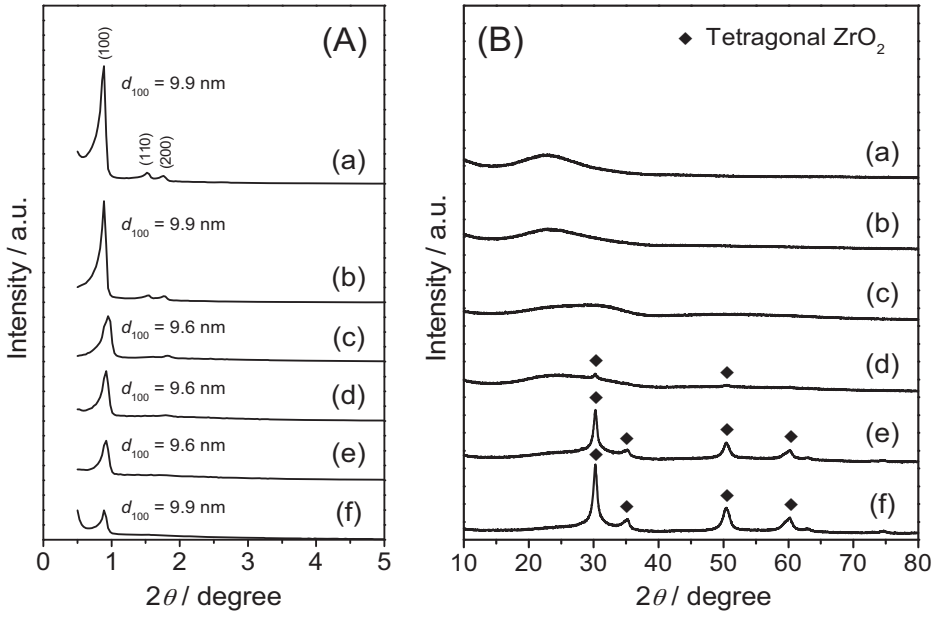

Fig. 1. (A) Small-angle and (B) wide-angle XRD patterns of (a) parent SBA-15 and ZrO_2/SBA-15 with varied ZrO_2 content; (b) 10, (c) 20, (d) 35, (e) 50 and (f) 60 wt% in the initial gel.

Table 2
CTH reaction of ML to GVL with 2-propanol as a hydrogen donor[a].

Entry	Catalyst	ZrO_2 content (wt%)	Conv. (%)	GVL yield (%)	GVL production rate (mmol/g-ZrO_2/h)
1	ZrO_2(10)/SBA-15	9.8	>99.5	91	15.2
2	ZrO_2(20)/SBA-15	19.4	98	89	14.8
3	ZrO_2(35)/SBA-15	32.7	84	76	12.7
4	ZrO_2(50)/SBA-15	49.7	70	62	10.3
5	ZrO_2(60)/SBA-15	59.2	61	55	9.2
6	ZrO_2(10)/MCM-41	9.7	98	89	14.8
7	ZrO_2(10)/SiO_2	9.6	98	87	14.5
8	ZrO_2	100	55	53	8.8
9	SBA-15	–	no reaction		

[a] Reaction conditions: catalyst (40 mg as ZrO_2), ML (2 mmol), 2-PrOH (10 mL), 150 °C, Ar (1.0 MPa), 3 h.

3.2. Investigation of local structure of Zr species

The local structure of the Zr atoms supported on silica supports were investigated by X-ray absorption measurement. Fig. 4(A) and (B) shows normalized X-ray absorption near-edge structure (XANES) spectra at the Zr K-edge and the corresponding RDFs of a series of ZrO_2/SBA-15 samples, together with pure monoclinic ZrO_2 as a reference. As shown in Fig. 4(A), the peak positions of the edge were invariant for all the samples. Focusing on the edge-top region, the intensity of the peak at around 18018 eV increased

Please cite this article in press as: Y. Kuwahara, et al., Catalytic transfer hydrogenation of biomass-derived levulinic acid and its esters to γ-valerolactone over ZrO_2 catalyst supported on SBA-15 silica, Catal. Today (2016), http://dx.doi.org/10.1016/j.cattod.2016.05.016

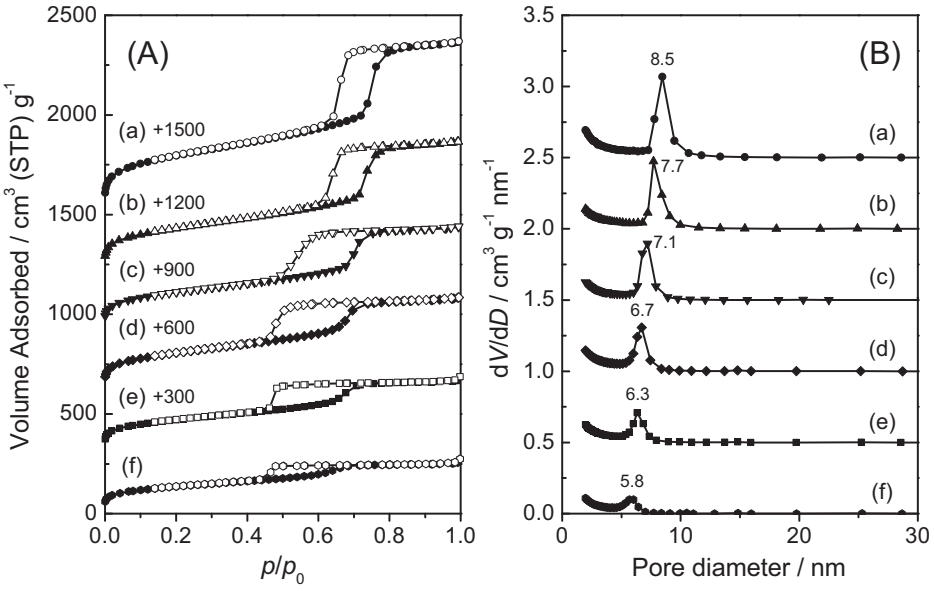

Fig. 2. (A) Nitrogen adsorption-desorption isotherms and (B) the corresponding pore size distribution curves of (a) parent SBA-15 and ZrO_2/SBA-15 with varied ZrO_2 content; (b) 10, (c) 20, (d) 35, (e) 50 and (f) 60 wt% in the initial gel. Filled and empty symbols in the left represent adsorption and desorption branches, respectively.

gradually and the peak at around 18025 eV adversely became less pronounced as the ZrO_2 loading in ZrO_2/SBA-15 samples increased. Interestingly, the latter peak was hardly observed in the spectrum of pure ZrO_2 with heptahedral coordination geometry [46]. The origin of the latter peak has been ascribed to the Zr atoms stabilized in a distorted polyhedron with reduced Zr—O bond distances [47]. These features indicate that the Zr species supported on SBA-15 silica are in the 4+ oxidation state in distorted coordination geometry.

In the RDFs, the peaks corresponding to Zr—O and Zr···Zr bonds were observed at around r = 1.5–1.6 and 3.0 Å (the phase shift

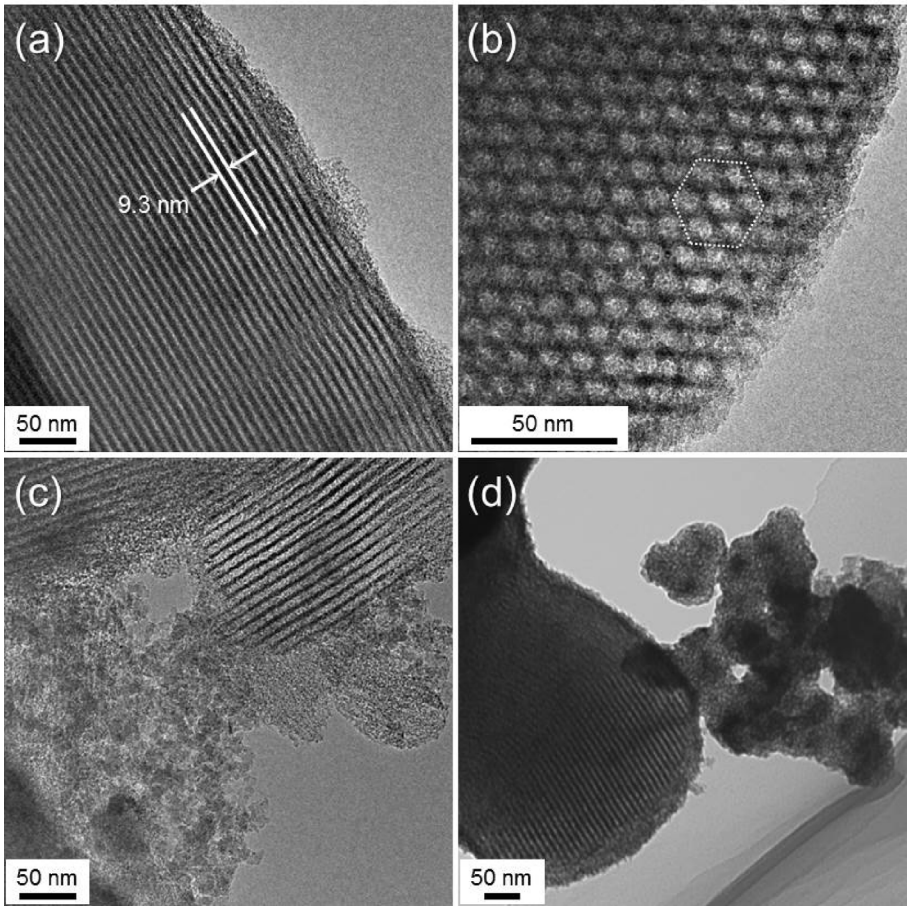

Fig. 3. TEM images of ZrO_2(10)/SBA-15 ((a) side-view, (b) top-view), (c) ZrO_2(35)/SBA-15 and (d) ZrO_2(60)/SBA-15.

Please cite this article in press as: Y. Kuwahara, et al., Catalytic transfer hydrogenation of biomass-derived levulinic acid and its esters to γ-valerolactone over ZrO_2 catalyst supported on SBA-15 silica, Catal. Today (2016), http://dx.doi.org/10.1016/j.cattod.2016.05.016

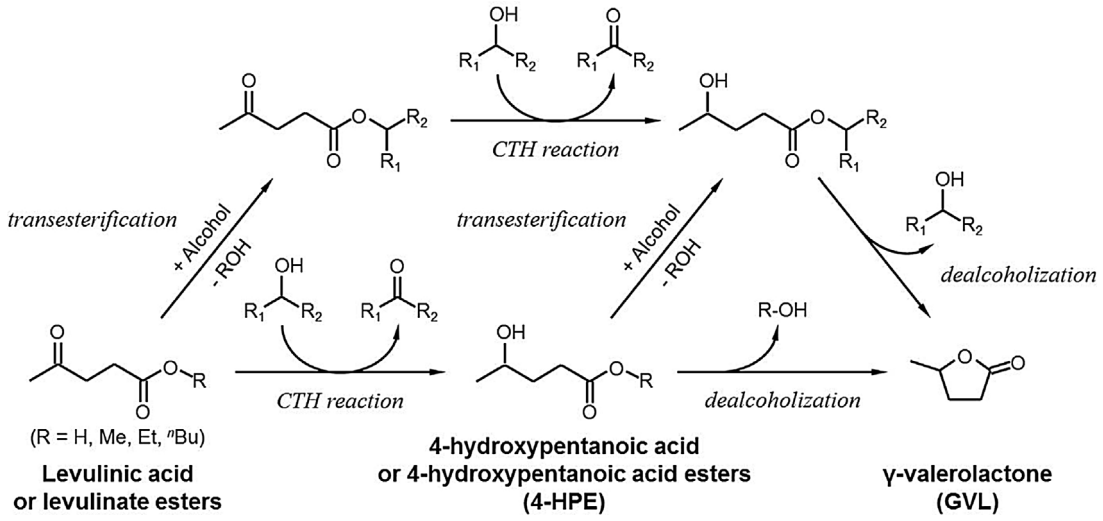

Scheme 1. Catalytic transfer hydrogenation (CTH) of levulinic acid and its esters using alcohol as a H-donor.

Table 3
Zr K-edge EXAFS curve-fitting parameters of silica-supported ZrO_2 catalysts[a].

Sample	ZrO_2 content (wt%)	Shell	C.N.[b]	R[c] (Å)	$\Delta\sigma^2$[d] (Å^2)
ZrO_2(10)/SBA-15	9.8	Zr—OZr···Zr	4.500.93	2.1213.401	0.0620.043
ZrO_2(20)/SBA-15	19.4	Zr—OZr···Zr	5.171.03	2.1213.404	0.0600.052
ZrO_2(35)/SBA-15	32.7	Zr—OZr···Zr	6.612.88	2.1283.425	0.0810.088
ZrO_2(50)/SBA-15	49.7	Zr—OZr···Zr	7.153.16	2.1283.693	0.0810.088
ZrO_2(60)/SBA-15	59.2	Zr—OZr···Zr	7.093.31	2.1203.691	0.0720.086
ZrO_2(10)/MCM-41	9.7	Zr—OZr···Zr	4.911.25	2.1213.415	0.0620.050
ZrO_2(10)/SiO_2	9.6	Zr—OZr···Zr	5.511.61	2.1223.431	0.0600.059
ZrO_2	100	Zr—OZr···Zr	7 7	2.1603.460	N.D. N.D.

[a] k^3-weighted EXAFS, $3.0 \le k(Å^{-1}) \le 13.0$.
[b] Average coordination number.
[c] Average atomic distance.
[d] Debye–Waller factor.

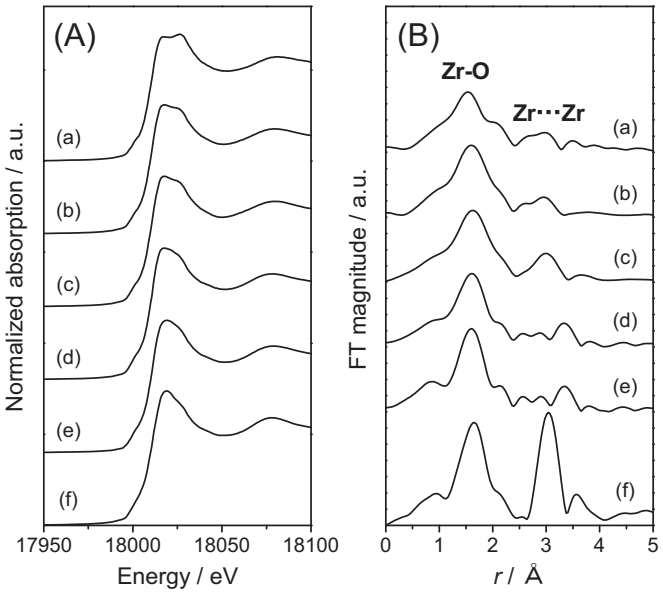

Fig. 4. (A) Zr K-edge XANES spectra and (B) radial distribution functions of ZrO_2/SBA-15 with varied ZrO_2 content ((a) 10, (b) 20, (c) 35, (d) 50 and (e) 60 wt% in the initial gel) and (f) monoclinic ZrO_2 as a reference sample.

uncorrected), respectively (Fig. 4(B)). Distinct changes of RDFs were found with the variation of the chemical composition of ZrO_2/SBA-15 samples; the position of the first shell (Zr—O) shifted to shorter distance side with a significant decrease in the FT magnitude as the ZrO_2 content in the samples decreased. In fact, it was confirmed by curve-fitting analysis that the coordination numbers (C.N.) and the interatomic distance (R) of the first Zr—O shell for the supported ZrO_2 samples were apparently smaller than those for bulk ZrO_2 (Table 3); as for ZrO_2(10)/SBA-15, the C.N. and R of the first Zr—O shell were determined to be 4.50 and 2.12 Å, respectively, whereas those of bulk ZrO_2 were 7 and 2.16 Å [46], elucidating that the highly-dispersed Zr atoms supported on SBA-15 are in low-coordination state with reduced Zr—O bond distances. In comparison, the C.N. of the Zr—O shell was found to be ca. 7.1 at higher ZrO_2 loading levels (50–60 wt%), which is almost similar to that of bulk ZrO_2, again indicating the formation of aggregated ZrO_2 crystals at higher ZrO_2 loading levels. Furthermore, the FT magnitude of the second shell (Zr···Zr) for the supported ZrO_2 samples was considerably damped compared to that for bulk ZrO_2; as the ZrO_2 content increased from 9.8 to 59.2 wt%, the C.N. for the Zr···Zr shell drastically changed from 0.93 to 3.31, which are quite smaller than that for bulk ZrO_2 (C.N. = 7). In particular, ZrO_2(10)/SBA-15 provided the lowest C.N. value for the Zr···Zr shell (0.93) compared with other types of silica-supported ZrO_2 samples (1.25 for ZrO_2(10)/MCM-41 and 1.61 for ZrO_2(10)/SiO_2) despite the same ZrO_2 content, which is probably due to the difference in surface area effective for anchoring Zr atoms. It is also worth noting that ZrO_2(50)/SBA-15 and ZrO_2(60)/SBA-15 exhibited the signals assignable to Zr···Zr shell at r = 3.34 Å (R = 3.69 Å), which coincided with that of tetragonal ZrO_2 (R = 3.63 Å) [46]. This result is in good agreement with the XRD result (see Fig. 1). These XAFS results can well explain the dispersion state of the Zr atoms stabilized on

Please cite this article in press as: Y. Kuwahara, et al., Catalytic transfer hydrogenation of biomass-derived levulinic acid and its esters to γ-valerolactone over ZrO_2 catalyst supported on SBA-15 silica, Catal. Today (2016), http://dx.doi.org/10.1016/j.cattod.2016.05.016

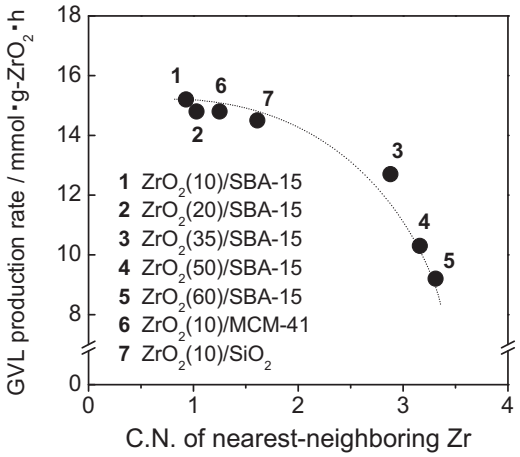

Fig. 5. Relationship between coordination numbers (C.N.) of nearest-neighboring Zr atoms and catalytic activities in the CTH reaction of ML with 2-propanol over silica-supported ZrO_2 catalysts.

silicas, *i.e.* the Zr atoms are present as highly-dispersed species with low-coordination geometry at lower ZrO_2 level, and are present as agglomerated species at higher ZrO_2 level.

The thus calculated C.N. values could be used as a good indicator associated the catalytic activity in the CTH reaction. Fig. 5 shows the plot of the catalytic activities against the C.N. of nearest-neighboring Zr atoms of the series of silica-supported ZrO_2 samples, which provided a more distinct correlation rather than the ones plotted against the other textural parameters. This correlation corroborates the idea that the highly-dispersed Zr^{4+}-oxide species with a low-coordination state anchored on silica surface is the dominant active species for the CTH reaction, where high-surface-area silica support provides a suitable environment for generating such active species.

3.3. Investigation of acid-base properties

To investigate the catalytic role of the Zr^{4+}-oxide species, TPD measurement was performed using NH_3 and CO_2 as probe molecules. Normalized NH_3 and CO_2-TPD profiles of $ZrO_2(10)$/SBA-15, bulk ZrO_2 and normal SBA-15 samples are shown in Fig. 6(A) and (B), respectively. In NH_3-TPD profiles, $ZrO_2(10)$/SBA-15 exhibited a desorption peak positioned at 140 °C which is attributed to weak acid sites and a broad desorption peak in the range of 200–400 °C which is assigned to medium acid sites, whereas normal SBA-15 exhibited almost no signals. The total amount of acid sites increased in the following order: SBA-15 (0.067 mmol/g) < ZrO_2 (0.381 mmol/g) < $ZrO_2(10)$/SBA-15 (0.784 mmol/g). A similar trend was observed in CO_2-TPD profiles. $ZrO_2(10)$/SBA-15 exhibited a desorption peak at around 225 °C which can be assigned to medium basic sites, whereas normal SBA-15 exhibited almost no TPD signals and bulk ZrO_2 exhibited a peak at lower temperature region (around 155 °C). The total amount of basic sites increased in the order of SBA-15 (0.047 mmol/g) < ZrO_2 (0.228 mmol/g) < $ZrO_2(10)$/SBA-15 (0.259 mmol/g). These results demonstrate that the Zr species in $ZrO_2(10)$/SBA-15 catalyst bear both acid and basic properties stronger than those in bulk ZrO_2. Topologically-different counterparts, $ZrO_2(10)/SiO_2$ and $ZrO_2(10)$/MCM-41, exhibited similar or even weaker acid/base properties; however, the basic strength of $ZrO_2(10)$/SBA-15 was, interestingly, found to be the highest among the samples tested (for TPD profiles of $ZrO_2(10)$/MCM-41 and $ZrO_2(10)/SiO_2$, see Fig. D). While the cause of the creation of such unusual stronger basic site on the surface of SBA-15 silica has not fully understood yet, this might be the one of the reasons why $ZrO_2(10)$/SBA-15 provided the highest activity in the CTH reaction.

Poisoning experiments were also carried out by introducing two different external additives, pyridine and benzoic acid, into the reaction system in order to elucidate the catalytic role of the above-mentioned acid/base properties. Fig. 7 shows the effects of the two additives on the catalytic activity of $ZrO_2(10)$/SBA-15 catalyst in the CTH reaction of ML to GVL, where pyridine and benzoic acid strongly interact with acidic and basic sites of the catalyst, respectively. As shown in Fig. 7, the addition of benzoic acid drastically reduced the activity, while the addition of pyridine had little impact on the activity, being consistent with the result by Sun and Lin et al. [39,40]. This result reveals that the CTH reaction of ML to GVL is primarily dominated by basic property of the Zr-oxide species and acid property have little involvement in the reaction.

3.4. In-situ *FTIR study*

To obtain insights about the reaction mechanism, *in-situ* FTIR measurement was performed using 2-propanol as a probe molecule. The measurement was performed at the temperature higher than the batch reaction conditions, 180 °C, to obtain sufficient IR intensity. Fig. 8 shows *in-situ* FTIR difference spectra of the adsorption complexes formed by the adsorption of 2-propanol on $ZrO_2(10)$/SBA-15 as a function of flushing time in He flow at 180 °C. The IR spectrum taken at 0 min showed a negative band appeared at 3735 cm^{-1}, which is attributed to the loss of surface —OH groups due to the interaction with 2-propanol, as well as absorption bands typical of free 2-propanol molecules; ν(OH): 3653 cm^{-1}, $\nu(CH_3)_{as}$: 2980 cm^{-1}, $\nu(CH_3)_s$: 2890 cm^{-1}, $\delta(CH_3)_{as}$, 1462 cm^{-1}, $\delta(CH_3)_s$: 1386 cm^{-1} [48]. The gradual decay of the absorption bands at 3653, 2980, 2890, 1462 and 1386 cm^{-1} after He flushing represents the desorption of 2-propanol molecules weakly adsorbed on the surface. However, the bands assignable to C—H stretching/bending vibrations still remained even after the He flow for 1 h at 180 °C. Unfortunately, the bands assignable to C—O stretching vibration (typically seen at around 1163 cm^{-1}) were not observed due to the significant overlapping with the bands of siloxane network of silica support. Furthermore, an absorption band assignable to the C=O stretching vibration mode appeared at 1685 cm^{-1}, which appreciably shifted to lower wavenumbers compared to that of free acetone molecule, suggesting the presence of acetone molecules strongly adsorbed on the surface [48]. These results indicate that metal-bound 2-propoxide species are formed *via* a deprotonation of 2-propanol, part of which is then transformed to acetone *via* a hydride elimination from β-position.

Based on the *in-situ* FTIR results together with the results of the above catalyst characterizations, a plausible reaction mechanism of the CTH reaction is proposed as follows (Scheme 2). First step is the interaction of alcohol with the Zr-related acid–base site (unsaturated Zr^{4+}—O^{2-} pairs), where alcohol is adsorbed on the basic Zr site (Zr—OH species) and dissociated to form the corresponding Zr-bound alkoxide (Step 1). The carbonyl group of levulinate ester is then coordinated to the Zr site, probably due to the electrostatic interaction between electron-rich oxygen atoms in the carbonyl group and the electron-deficient Zr-related Lewis acid site, while this is not a rate-determining step, and subsequently forms a six-membered ring transition state (Step 2). The β-hydride of the Zr-bound alkoxide attacks the carbonyl group of levulinate ester to yield Zr-bound 4-hydroxypentanoic acid ester (4-HPE) species and new carbonyl compound corresponding to the alcohol (Step 3). Subsequently, the carbonyl byproduct is released (Step 4) and the Zr-bound 4-HPE species are displaced by another alcohol to regenerate the Zr-bound alkoxide species (Step 5), thus the catalytic cycle is completed. The released 4-HPE is thermodynamically unstable as rarely being detected by a GC analysis (see also Table 4), therefore,

Please cite this article in press as: Y. Kuwahara, et al., Catalytic transfer hydrogenation of biomass-derived levulinic acid and its esters to γ-valerolactone over ZrO_2 catalyst supported on SBA-15 silica, Catal. Today (2016), http://dx.doi.org/10.1016/j.cattod.2016.05.016

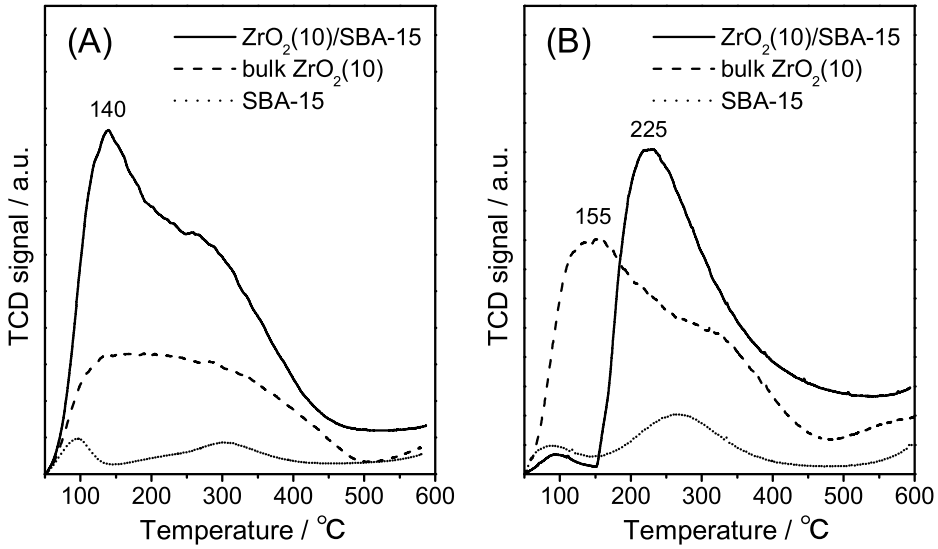

Fig. 6. (A) NH_3 and (B) CO_2 TPD profiles of SBA-15, ZrO_2(10)/SBA-15 and bulk ZrO_2 samples. TCD signals were normalized by the weight of the samples used in each experiment.

Table 4
Scope of substrates and alcohols for the production of GVL over ZrO_2(10)/SBA-15 catalyst[a].

Entry	Substrate[e]	Alcohol	Conv. (%)	Selectivity[f] (%)				GVL yield (%)
				GVL	Trans	Trans + H	Others	
1[b]	ML	MeOH	4.7	30	0	0	70	1.4
2	ML	EtOH	98	42	51	0	7	41
3	ML	1-PrOH	98	40	54	4	2	39
4	ML	2-PrOH	>99.5	90	6	4	0	91
5[c]	ML	2-PrOH	>99.9	95	1	4	0	95
6	ML	2-BuOH	99	90	4	6	0	89
7	ML	CyOH	97	91	1	6	2	88
8	EL	EtOH	15	93	0	0	7	14
9[d]	EL	EtOH	65	92	0	0	8	60
10	EL	2-PrOH	97	94	0	6	0	91
11	BL	2-PrOH	81	88	6	6	0	71
12	LA	2-PrOH	>99.9	90	5	5	0	90

[a] Reaction conditions: catalyst (40 mg as ZrO_2), substrate (2 mmol), alcohol (10 mL), 150 °C, Ar (1.0 MPa), 3 h.
[b] At 90 °C.
[c] At 6 h of reaction.
[d] At 21 h of reaction.
[e] ML = methyl levulinate, EL = ethyl levulinate, BL = *n*-butyl levulinate, LA = levulinic acid.
[f] Trans = transesterification product. Trans + H = transesterification and hydrogenated product. Others = hydrogenated product + unknown product.

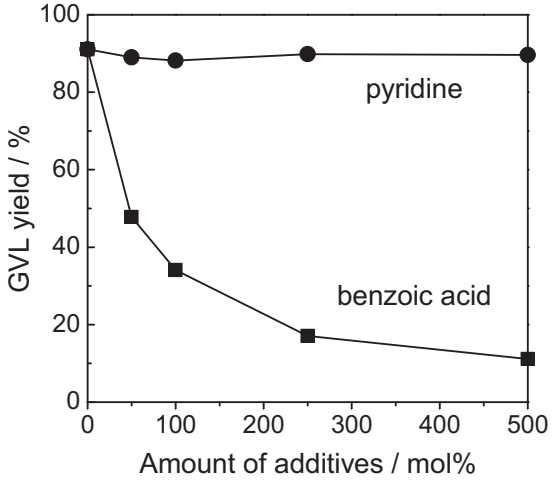

Fig. 7. Effect of addition of pyridine and benzoic acid on the catalytic activity of ZrO_2(10)/SBA-15 catalyst. Reaction conditions: catalyst (40 mg as ZrO_2), ML (2 mmol), 2-PrOH (10 mL), additive (0–500 mol%), 150 °C, Ar (1.0 MPa), 3 h.

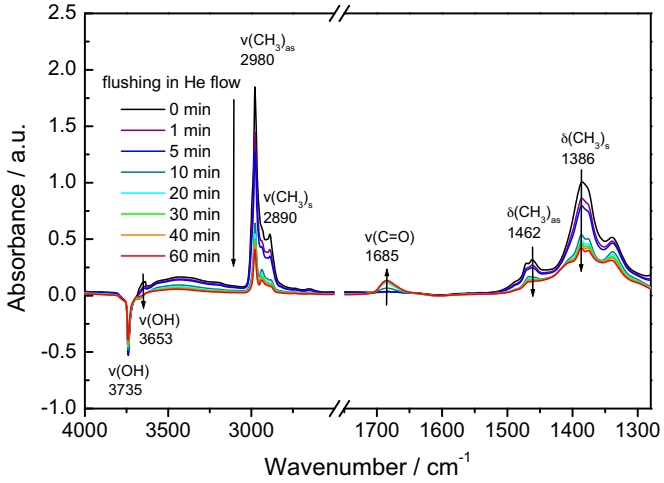

Fig. 8. *In-situ* FTIR difference spectra of the adsorption complexes formed by the adsorption of 2-propanol on ZrO_2(10)/SBA-15 as a function of flushing time in He flow at 180 °C.

Please cite this article in press as: Y. Kuwahara, et al., Catalytic transfer hydrogenation of biomass-derived levulinic acid and its esters to γ-valerolactone over ZrO_2 catalyst supported on SBA-15 silica, Catal. Today (2016), http://dx.doi.org/10.1016/j.cattod.2016.05.016

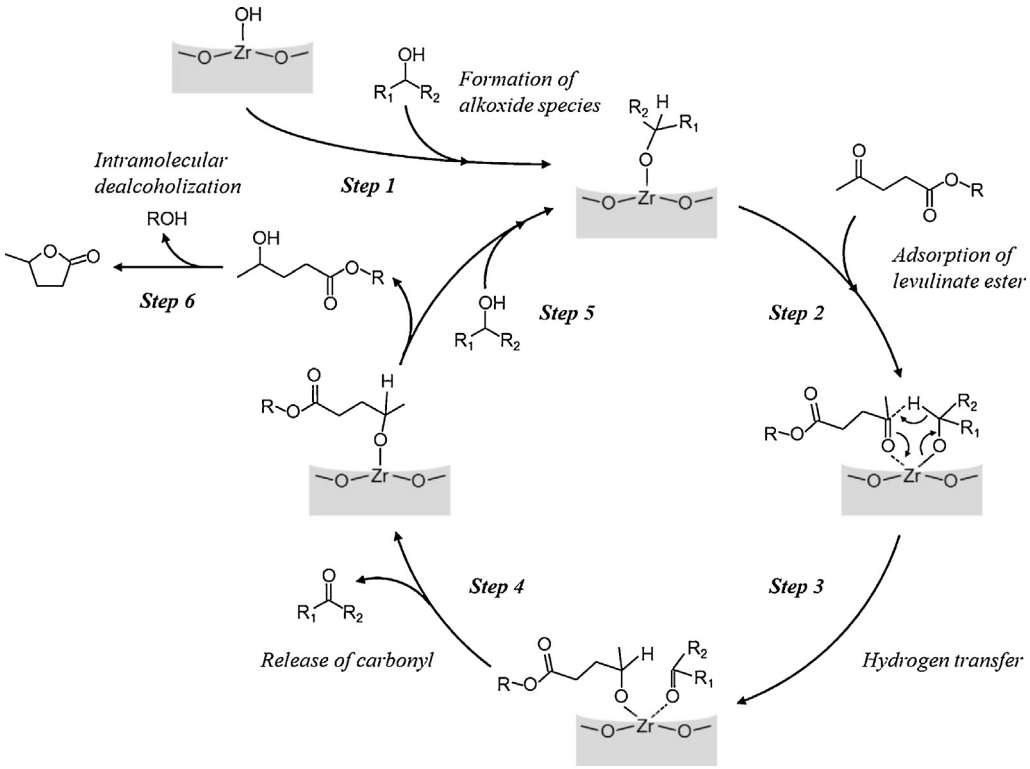

Scheme 2. Proposed reaction mechanism of the catalytic transfer hydrogenation (CTH) of levulinate esters over silica-supported ZrO_2 catalyst using alcohol as a H-donor.

it readily undergoes intramolecular dealcoholization to give GVL together with the formation of the equimolar amount of alcohol (Step 6) [49]. Since each step in this reaction is reversible, the reaction rate is controlled by the concentrations and thermodynamic properties of the products and intermediates. Because the rate of step 6 is very fast, the reaction equilibrium tends to incline to the 4-HPE formation, thereby a high GVL yield can be achieved. The rate determining step in this process must be step 1 where the Zr-related basic site (Zr—OH species) plays a vital role for abstracting protons from alcohols [40,50]. This assumption can be elucidated by the experiments using ZrO_2(10)/SBA-15 pre-treated at different temperatures. The catalytic activity significantly decreased when it was pre-treated at temperatures higher than 400 °C, and showed a continuous decrease as the pre-treatment temperature increased (Fig. E). This trend coincided well with that observed in the TG analysis, which showed a distinct weight loss assignable to the removal of surface —OH groups over 330 °C (Fig. E). Considering the fact that crystallinity and porous structures were hardly changed upon pre-treatment up to 800 °C, the observed activity loss should be attributed to the removal of Zr—OH groups which triggers the CTH reaction. One of the reasons why ZrO_2(10)/SBA-15 provided the highest activity in the CTH reaction might be attributed to the creation of stronger basic sites as discussed above.

3.5. Scope of substrates and alcohols

The alcohol, which works as a H-donor as well as a reaction solvent, plays an important role in the CTH process. Herein, various primary and secondary alcohols were evaluated as the H-donors in the CTH reaction of ML using ZrO_2(10)/SBA-15 as a catalyst (Table 4). Among various alcohols examined, secondary alcohols such as 2-propanol, 2-butanol and cyclohexanol worked as efficient H-donors, which afforded similar GVL yields (88–91%) at 3 h of reaction with more than 90% selectivity (Entries 4, 6, 7). Prolonging reaction time to 6 h led to an increased GVL yield of 95% (Entry 5). In contrast, use of primary alcohols such as ethanol and 1-propanol resulted in moderate GVL yields (39–41%) (Entries 2, 3), affording the corresponding transesterification products as main products. This is because the β-hydride elimination from such Zr-bound ethoxide/propoxide species is difficult to take place (for reaction kinetics data, see Fig. F) [39,40].

GVL could be synthesized from other levulinate derivatives, including ethyl levulinate (EL), butyl levulinate (BL) and levulinic acid (LA), using 2-propanol as a H-donor (Entries 10–12). The GVL production rate increased in the order of BL < EL < LA = ML (for reaction kinetics data, see Fig. F), demonstrating a substantial impact of the alkyl chain length of the ester groups, which might be associated with the dealcoholization step (Step 6 in Scheme 2). In addition, combination of EL and ethanol was possible for the production of GVL, although the reaction rate was quite low; 14% and 60% GVL yields were obtained after 3 and 21 h of reaction (Entries 8 and 9). EL can be produced from biomass through alcoholysis of sugars in ethanol media, which ideally affords an ethanol solution containing EL (as well as the equimolar amount of ethyl formate). A direct use of the ethanol media as a H-donor in the following CTH process will be a promising strategy for GVL production, because several energy-consuming steps associated with isolation and purification can be skipped. This result opens up a possibility for the establishment of a simple and low-cost GVL production from biomass, for which ZrO_2(10)/SBA-15 catalyst can be a viable option, although a further improvement of catalytic performance is needed before substantiating this technology.

3.6. Reusability of catalyst

To assess the reusability and stability of the catalyst, ZrO_2(10)/SBA-15 and bulk ZrO_2 catalysts were subjected to five successive catalytic cycles in the CTH reaction of ML with 2-propanol under the standard reaction conditions (*i.e.*, 150 °C, Ar 1.0 MPa, 3 h). As shown in Fig. 9, ZrO_2(10)/SBA-15 was at least five times reusable with keeping most of its activity (91% → 76%

Please cite this article in press as: Y. Kuwahara, et al., Catalytic transfer hydrogenation of biomass-derived levulinic acid and its esters to γ-valerolactone over ZrO_2 catalyst supported on SBA-15 silica, Catal. Today (2016), http://dx.doi.org/10.1016/j.cattod.2016.05.016

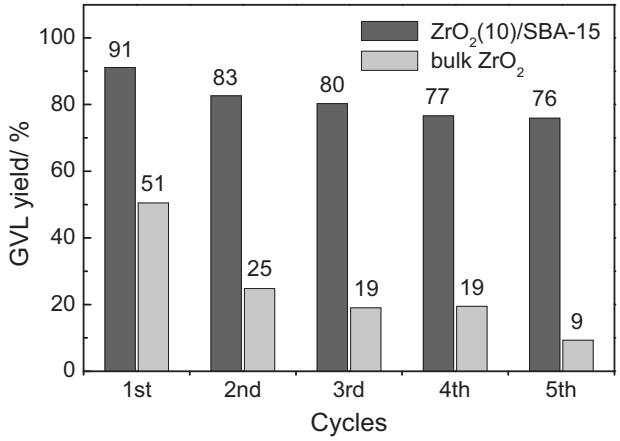

Fig. 9. Catalyst reusability tests of ZrO_2(10)/SBA-15 and bulk ZrO_2 catalysts.

GVL yields in fifth catalytic cycle), while bulk ZrO_2 showed a significant activity reduction (51% → 9% GVL yields in fifth catalytic cycle). Structural analysis of the spent catalyst by means of XRD, N_2 physisorption and TEM measurements revealed that the crystalline/porous structures of the catalyst were mostly retained even after five catalytic cycles (see Fig. G). In addition, the loss of active Zr species was not observed upon the reaction. These results demonstrate that ZrO_2(10)/SBA-15 catalyst acts as more efficient, reusable heterogeneous catalyst for the CTH reaction of levulinate esters to give GVL compared to the conventional bulk ZrO_2. Thermogravimetric (TG) analysis of the spent catalyst indicated a deposition of appreciable amount (ca. 5 wt%) of carbonaceous species on the catalyst surface after its use (see Fig. G). Considering the reaction mechanism proposed above, the detected organic residue should originate from the surface-bound alkoxide and 4-HPE species accumulated on the surface, which likely prevent the access of levulinate esters and alcohols to the active Zr sites and thus retard the overall reaction rate. The observed difference in the catalyst reusability between ZrO_2(10)/SBA-15 and bulk ZrO_2 catalysts might be attributed to the different chemical environment of Zr species, *i.e.* the highly-dispersed Zr species stabilized on high-surface-area SBA-15 may suppress over-accumulation of organic species owing to the site separation effect, leaving spaces where the reactants can access, whereas bulk ZrO_2 with low surface area causes an easy accumulation of organic species due to the proximity of each active site.

4. Conclusions

In this study, a series of ZrO_2 catalysts supported on mesoporous SBA-15 silica were prepared and examined in the CTH reaction of biomass-derived levulinic acid and its esters to produce GVL using several alcohols as hydrogen donors. Catalytic results, combined with structural analyses using XRD, N_2 physisorption, TEM and Zr K-edge XAFS, demonstrated that the GVL production rate correlates well with the dispersion state of Zr atoms supported on silicas rather than other textural properties, more specifically, the highly-dispersed Zr^{4+}-oxide species with low-coordination geometry is the dominant active species. Of the catalysts examined, ZrO_2(10)/SBA-15 with 10 wt% ZrO_2 content was found to be the most promising catalyst combining a high catalytic activity, reusability and stability, which far outperformed those of the conventional bulk ZrO_2 catalyst. Furthermore, based on the comparative experiments, combined with detailed characterizations using NH_3/CO_2-TPD and *in-situ* FTIR, a plausible reaction mechanism was proposed, where basic Zr—OH site triggers the CTH reaction involving a six-member ring transition state. The catalyst developed in this study offers a simple, reusable, noble-metal-free catalytic system that enables efficient production of a valuable platform molecule, GVL, from biomass-derived levulinic acid and its esters.

Acknowledgements

This study was financially supported by the National Institute of Advanced Industrial Science and Technology (AIST). A part of this work was also supported by the Grant-in-Aid from Frontier Research Base for Global Young Researchers, Osaka University and the Grant-in-Aid for Scientific Research (KAKENHI) from the Japan Society for the Promotion of Science (JSPS) (No. 15K18270). The synchrotron radiation experiments were performed at the BL01B1 beam line at SPring-8 with the approval of JASRI (No. 2014A1045).

Appendix A. Supplementary data

Supplementary data associated with this article can be found, in the online version, at http://dx.doi.org/10.1016/j.cattod.2016.05.016.

References

[1] A. Corma, S. Iborra, A. Velty, Chem. Rev. 107 (2007) 2411–2502.
[2] J.N. Chheda, G.W. Huber, J.A. Dumesic, Angew. Chem. Int. Ed. 46 (2007) 7164–7183.
[3] D.M. Alonso, J.Q. Bond, J.A. Dumesic, Green Chem. 12 (2010) 1493–1513.
[4] J.J. Bozell, G.R. Petersen, Green Chem. 12 (2010) 539–554.
[5] M.J. Climent, A. Corma, S. Iborra, Green Chem. 13 (2011) 520–540.
[6] M.J. Climent, A. Corma, S. Iborra, Green Chem. 16 (2014) 516–547.
[7] J.C. Serrano-Ruiz, R. Luque, A. Sepúlveda-Escribano, Chem. Soc. Rev. 40 (2011) 5266–5281.
[8] I.T. Horváth, H. Mehdi, V. Fábos, L. Boda, L.T. Mika, Green Chem. 10 (2008) 238–242.
[9] D.M. Alonso, S.G. Wettstein, J.A. Dumesic, Green Chem. 15 (2013) 584–595.
[10] J.M.R. Gallo, D.M. Alonso, M.A. Mellmer, J.A. Dumesic, Green Chem. 15 (2013) 85–90.
[11] D. Wang, S.H. Hakim, D. Martin Alonso, J.A. Dumesic, Chem. Commun. 49 (2013) 7040–7042.
[12] L.E. Manzer, Appl. Catal. A 272 (2004) 249–256.
[13] J.-P. Lange, J.Z. Vestering, R.J. Haan, Chem. Commun. (2007) 3488–3490.
[14] J.C. Serrano-Ruiz, D. Wang, J.A. Dumesic, Green Chem. 12 (2010) 574–577.
[15] F.M.A. Geilen, B. Engendahl, A. Harwardt, W. Marquardt, J. Klankermayer, W. Leitner, Angew. Chem. Int. Ed. 49 (2010) 5510–5514.
[16] J.Q. Bond, D.M. Alonso, D. Wang, R.M. West, J.A. Dumesic, Science 327 (2010) 1110–1114.
[17] D.J. Braden, C.A. Henao, J. Heltzel, C.C. Maravelias, J.A. Dumesic, Green Chem. 13 (2011) 1755–1765.
[18] X. Hu, C.-Z. Li, Green Chem. 13 (2011) 1676–1679.
[19] Z. Wu, S. Ge, C. Ren, M. Zhang, A. Yip, C. Xu, Green Chem. 14 (2012) 3336–3343.
[20] A. Démolis, N. Essayem, F. Rataboul, ACS Sustainable Chem. Eng. 2 (2014) 1338–1352.
[21] K.-i. Tominaga, A. Mori, Y. Fukushima, S. Shimada, K. Sato, Green Chem. 13 (2011) 810–812.
[22] L. Peng, L. Lin, J. Zhang, J. Shi, S. Liu, Appl. Catal. A 397 (2011) 259–265.
[23] X. Hu, Y. Song, L. Wu, M. Gholizadeh, C.-Z. Li, ACS Sustainable Chem. Eng. 1 (2013) 1593–1599.
[24] Y. Kuwahara, T. Fujitani, H. Yamashita, Catal. Today 237 (2014) 18–28.
[25] Y. Kuwahara, W. Kaburagi, K. Nemoto, T. Fujitani, Appl. Catal. A 476 (2014) 186–196.
[26] P.P. Upare, J.-M. Lee, D.W. Hwang, S.B. Halligudi, Y.K. Hwang, J.-S. Chang, J. Ind. Eng. Chem. 17 (2011) 287–292.
[27] K. Yan, C. Jarvis, T. Lafleur, Y. Qiao, X. Xie, RSC Adv. 3 (2013) 25865–25871.
[28] K. Yan, T. Lafleur, G. Wu, J. Liao, C. Ceng, X. Xie, Appl. Catal. A 468 (2013) 52–58.
[29] L. Deng, J. Li, D.-M. Lai, Y. Fu, Q.-X. Guo, Angew. Chem. Int. Ed. 48 (2009) 6529–6532.
[30] Z.-p. Yan, L. Lin, S. Liu, Energy Fuels 23 (2009) 3853–3858.
[31] M.G. Al-Shaal, W.R.H. Wright, R. Palkovits, Green Chem. 14 (2012) 1260–1263.
[32] A.M.R. Galletti, C. Antonetti, V. De Luise, M. Martinelli, Green Chem. 14 (2012) 688–694.
[33] J.M. Nadgeri, N. Hiyoshi, A. Yamaguchi, O. Sato, M. Shirai, Appl. Catal. A 470 (2014) 215–220.
[34] Y. Kuwahara, Y. Magatani, H. Yamashita, Catal. Today 258 (Part (2)) (2015) 262–269.
[35] J. Deng, Y. Wang, T. Pan, Q. Xu, Q.-X. Guo, Y. Fu, ChemSusChem 6 (2013) 1163–1167.
[36] R.S. Assary, L.A. Curtiss, J.A. Dumesic, ACS Catal. 3 (2013) 2694–2704.
[37] Y. Kuwahara, W. Kaburagi, T. Fujitani, RSC Adv. 4 (2014) 45848–45855.

Please cite this article in press as: Y. Kuwahara, et al., Catalytic transfer hydrogenation of biomass-derived levulinic acid and its esters to γ-valerolactone over ZrO_2 catalyst supported on SBA-15 silica, Catal. Today (2016), http://dx.doi.org/10.1016/j.cattod.2016.05.016

[38] M. Chia, J.A. Dumesic, Chem. Commun. 47 (2011) 12233–12235.
[39] X. Tang, L. Hu, Y. Sun, G. Zhao, W. Hao, L. Lin, RSC Adv. 3 (2013) 10277–10284.
[40] X. Tang, H. Chen, L. Hu, W. Hao, Y. Sun, X. Zeng, L. Lin, S. Liu, Appl. Catal. B 147 (2014) 827–834.
[41] L. Bui, H. Luo, W.R. Gunther, Y. Román-Leshkov, Angew. Chem. Int. Ed. 52 (2013) 8022–8025.
[42] J. Wang, S. Jaenicke, G.-K. Chuah, RSC Adv. 4 (2014) 13481–13489.
[43] Y. Kuwahara, W. Kaburagi, T. Fujitani, Bull. Chem. Soc. Jpn. 87 (2014) 1252–1254.
[44] D. Zhao, J. Feng, Q. Huo, N. Melosh, G.H. Fredrickson, B.F. Chmelka, G.D. Stucky, Science 279 (1998) 548–552.
[45] C.T. Kresge, M.E. Leonowicz, W.J. Roth, J.C. Vartuli, J.S. Beck, Nature 359 (1992) 710–712.
[46] F. Meneghetti, E. Wendel, S. Mascotto, B.M. Smarsly, E. Tondello, H. Bertagnolli, S. Gross, CrystEngComm 12 (2010) 1639–1649.
[47] H. Jung, S.-M. Paek, J.-B. Yoon, J.-H. Choy, J. Porous Mater. 14 (2007) 369–377.
[48] M.I. Zaki, M.A. Hasan, L. Pasupulety, Langmuir 17 (2001) 4025–4034.
[49] J. Geboers, X. Wang, A.B. de Carvalho, R. Rinaldi, J. Mol. Catal. A 388-389 (2014) 106–115.
[50] Y. Zhu, S. Liu, S. Jaenicke, G. Chuah, Catal. Today 97 (2004) 249–255.

Please cite this article in press as: Y. Kuwahara, et al., Catalytic transfer hydrogenation of biomass-derived levulinic acid and its esters to γ-valerolactone over ZrO_2 catalyst supported on SBA-15 silica, Catal. Today (2016), http://dx.doi.org/10.1016/j.cattod.2016.05.016